PHYSICS OF FLUIDS VOLUME 16, NUMBER 7 JULY 2004

Stochastic coherent adaptive large eddy simulation method

Daniel E. Goldstein[a] and Oleg V. Vasilyev[b]
Mechanical Engineering Department, University of Colorado-Boulder, UCB 427, Boulder, Colorado 80309-0427

(Received 8 October 2003; accepted 24 February 2004; published online 2 June 2004)

In this paper we propose a novel approach called the stochastic coherent adaptive large eddy simulation (SCALES) method which takes advantage of both the coherent vortex simulation (CVS) and large eddy simulation (LES) methods. With the SCALES method a wavelet filter is applied to a turbulent field such that the maximum number of modes are resolved in the simulation, given the balance between computing resources and user defined acceptable simulation error. As with CVS, the wavelet thresholding filter will allow a SCALES simulation to resolve and ''track'' the coherent energetic structures in a turbulent flow field. The wavelet filter compression in SCALES will be substantially greater than the ''ideal'' wavelet compression used in CVS, making it cost effective for simulating high Re number flows. The SCALES methodology will simulate the most important modes given the resources available. Because of the higher wavelet compression the subgrid scales (SGS) in a SCALES simulation will contain both coherent and incoherent modes like with LES. In this work the SCALES method is presented for both velocity and vorticity space wavelet filtering. A novel coherency diagram of a turbulent field is introduced to present the physical relationships between direct numerical simulation and different large eddy capturing methods. In this work we show that with both LES filtering and SCALES filtering the residual SGS field contains both coherent and incoherent parts and that with both methodologies the total SGS dissipation is dominated by the coherent part of the SGS field. A possible implementation of the SCALES methodology for incompressible turbulent flows is also discussed. [DOI: 10.1063/1.1736671]

I. INTRODUCTION

The problem of simulating high Reynolds number (Re) turbulent flows of engineering and scientific interest would have been solved with the advent of direct numerical simulation (DNS) techniques if unlimited computing power, memory, and time could be applied to each particular problem. Yet, given the current and near future computational resources that exist and a reasonable limit on the amount of time an engineer or scientist can wait for a result, the DNS technique will not be useful for more than ''unit'' problems for the foreseeable future.[1,2] The high computational cost for the DNS of three-dimensional turbulent flows results from the fact that they have eddies of significant energy in a range of scales from the characteristic length scale of the flow all the way down to the Kolmogorov length scale. Because of the large disparity in scales that need to be fully resolved, the actual cost of doing a three-dimensional DNS scales as $Re^{9/4}$. Fortunately, because the eddies are localized in space and scale, there is a possibility of ''compressing'' the problem such that a simulation with a subset of the total modes captures the dynamics of the most energetic eddies.

Since computing power, memory, and time are all scarce resources, the problem of simulating turbulence has become one of how to abstract or simplify the complexity of the physics represented in the full Navier–Stokes (NS) equations in such a way that the ''important'' physics of the problem is captured at a lower cost. To do this, a portion of the modes of the turbulent flow field is approximated by a low order model that is cheaper than the full NS calculation. This model can then be used along with a numerical simulation of the ''important'' modes of the problem that cannot be well represented by the model. The decision of what part of the physics to model and what kind of model to use has to be based on what physical properties are considered ''important'' for the problem. It should be noted that ''nothing is free,'' so any use of a low order model will by definition lose some information about the original flow.

In an abstract sense the first question to address, when one is looking to develop a reduced order method for simulating turbulent flows, is how to determine what part of the physical system will be approximated with a low order model and what part will be simulated numerically. One choice is to average the behavior of the system over time. This technique is used in Reynolds averaged Navier–Stokes (RANS) simulations.[3] Another option is to treat the turbulent flow as a set of flow structures moving in a Lagrangian frame and track their interactions over time. This approach has been used in vortex simulation methods.[4] Yet another option is to simulate the flow on an adapted grid that is coarser than the grid necessary to represent the flow down to the Kolmogorov length scale. The goal of this type of method is to

[a]Electronic mail: Daniel.E.Goldstein@colorado.edu
[b]Author to whom correspondence should be addressed. Telephone: 303-492-4717; fax: 303-492-3498. Electronic mail: Oleg.Vasilyev@colorado.edu

resolve the energetic eddies that dominate the flow physics. Any coarsening of the grid, either locally or globally, implies that not all the modes or frequencies of the original flow are resolved. Therefore these ''missing'' modes will have to be modeled somehow. In this class of methods we will also include Galerkin[5,6] methods that approximate the problem on a reduced set of some basis functions. We will refer to this class of methods as eddy capturing methods.

The dominant method in the class of eddy capturing methods is large eddy simulation (LES). The motivation behind LES has been the recognition that the large scales of the turbulence often dominate mixing, heat transfer and other quantities of engineering interest, while the small scales are only of interest because of how they effect the large scales. The LES equations for incompressible flow, that describe the evolution of the large scale eddies in the flow field, can be written as

$$\frac{\partial \overline{u_i}}{\partial x_i}=0, \tag{1}$$

$$\frac{\partial \overline{u_i}}{\partial t}+\frac{\partial(\overline{u_i}\,\overline{u_j})}{\partial x_j}=-\frac{1}{\rho}\frac{\partial \overline{p}}{\partial x_i}+\nu\frac{\partial^2 \overline{u_i}}{\partial x_j \partial x_j}-\frac{\partial \tau_{ij}}{\partial x_j}, \tag{2}$$

where

$$\tau_{ij}=\overline{u_i u_j}-\overline{u_i}\,\overline{u_j} \tag{3}$$

and u_i is the velocity field, ρ is density, ν is kinematic viscosity, p is pressure, and $\overline{(\ )}$ represents spacial filtering. As a result of the filtering process the unresolved quantity τ_{ij}, commonly referred to as the subgrid scale (SGS) stress, is introduced. Note τ_{ij} is a function of the unfiltered field u_i. However, to realize the benefit of LES, a low order model for the SGS stress, which is based on the resolved quantities, is needed. In practice τ_{ij} can be modeled either deterministically or stochastically. Most current LES is done using purely deterministic models.[7–9] The current research efforts in LES largely involve finding improved SGS stress models for τ_{ij}.

In LES the filter that is used can be either an explicit filter or it can be implicitly defined by the computational grid. Either way LES uses a reduced computational grid that is capable of supporting (or representing) a subset of the modes of the actual flow. Current state of the art LES work uses nonuniformly stretched meshes or zonal grids[9–11] that are refined *a priori* to the geometry of the problem.

The problem with LES is that it resolves the large scale eddies instead of the coherent energetic eddies. It has been shown that the coherent vortices in a turbulent flow contain significant energy at all length scales from the characteristic length scale of the domain down to the Kolmogorov length scale.[12–15] In Ref. 16 a visual study of the physical structure of turbulence is presented. The authors conclude that the ''vorticity tubes, which seem to be the basic structure of three-dimensional homogeneous turbulence, involve all the scales of the flow.'' Because of this when a spectral cutoff filter is used with LES the small scale structures of the coherent energetic eddies are not resolved. Therefore these small scale energetic structures contained in the subgrid scales must be modeled. However, the hypothesis behind most LES subgrid scale models is that the subgrid scales being modeled have a generally universal character.[17,18] This issue will be further elaborated on in Sec. VII for LES with a sharp cutoff Fourier filter. It will be shown that the coherent portion of the subgrid scales is responsible for the majority of the subgrid scale dissipation. This result implies that LES models must model the stochastic and coherent parts of the SGS stress separately.

Another problem with LES is that the computational grid is commonly defined *a priori* based on the physics and geometry of the problem.[9,11,19] Yet in flow problems of engineering and scientific interest the large scales of interest often change over the domain of the problem and in time. As Pope states in his recent book on turbulence[18] ''the ideal numerical method for LES would include adaptive gridding to ensure automatically that the grid, and hence the filter, are everywhere sufficiently fine to resolve the energy-containing motions.'' This implies that there is a need for an eddy capturing method that is adaptive in time and space.

A relatively new method in the class of eddy capturing methods is the coherent vortex simulation[20] (CVS) method. CVS is based on the theory that a wavelet filter, when applied to a turbulent vorticity field, can decompose it into the resolved field that contains all the energetic coherent structures, or eddies, and the residual, or subgrid field, which is purely incoherent. In theory, if the subgrid field is purely incoherent white noise, the total SGS dissipation would be zero. Therefore the SGS stress model for a CVS simulation could be purely stochastic. The main problem with the CVS method is that ''ideal'' wavelet compression that results in a subgrid field that is purely incoherent can be difficult to determine on the fly during an actual simulation. Even if it can be found in a cost effective manner, it is also likely that the associated adaptive grid will be too fine to be cost effective for simulating high Re number flows.

In this paper we propose a novel approach called the stochastic coherent adaptive large eddy simulation (SCALES) method which takes advantage of both the CVS and LES methods. With the SCALES method a wavelet filter is applied to a turbulent field such that the maximum number of modes are resolved in the simulation, given the balance between computing resources and user defined acceptable simulation error. This will pick the most important modes to be simulated given the resources available. The wavelet filter compression in SCALES could be substantially greater than the ''ideal'' wavelet compression used in CVS making it cost effective for simulating high Re number flows. Because of the higher wavelet compression the SGS in a SCALES simulation will contain both coherent and incoherent modes like with LES. In this work the SCALES method is presented for both velocity and vorticity space wavelet filtering. The *a priori* results presented in this work use second generation lifted interpolating wavelets[21,22] of order 6 that we have used in previous work on a fully adaptive wavelet collocation solver[23–26] and that eventually will be used in the implementation of the SCALES method.

The rest of this paper is organized as follows: In Sec. II the theory of wavelets, and in particular second generation wavelets, will be briefly introduced. Then in Sec. III the

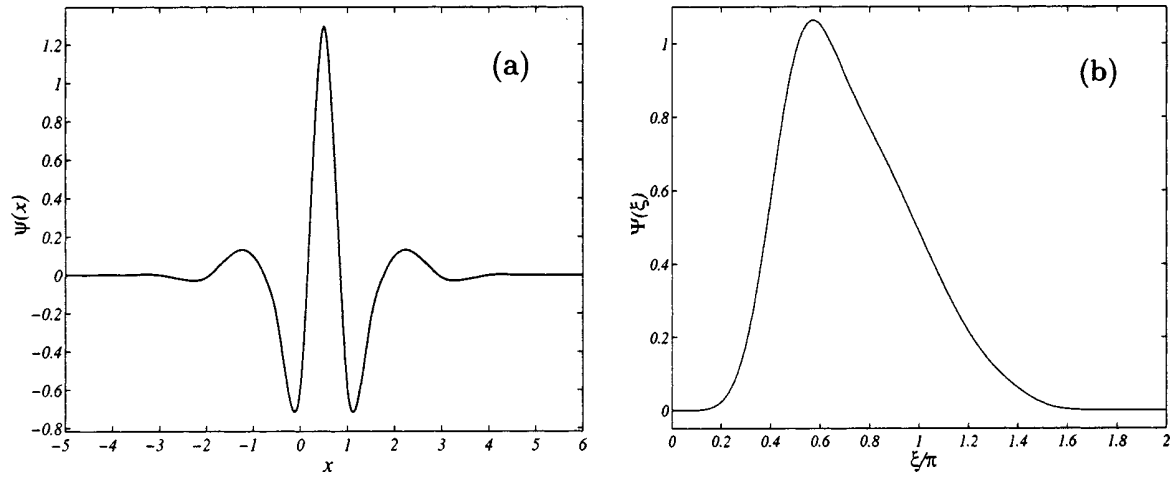

FIG. 1. Lifted interpolating wavelet ψ (a) and its Fourier transform $\Psi(\xi)$ (b).

wavelet thresholding filter will be presented in comparison to the more widely understood Fourier cutoff filter. Next in Sec. IV the CVS method will be discussed in more detail. This will be followed by Sec. V that will present a series of *a priori* tests where a wavelet thresholding filter and a Fourier cutoff filter are applied to an isotropic turbulence field and the statistical properties of the resolved and residual fields are compared. In Sec. VI a coherency diagram of a turbulent field is presented as a theoretical framework to compare different eddy capturing methods. Then in Secs. VII and VIII the stochastic coherent adaptive large eddy simulation (SCALES) method and the stochastic coherent large eddy simulation (SCLES) method (a nonadaptive version of the SCALES method) are presented. Conclusions and suggestions for future work are provided in Sec. IX.

II. WAVELET TRANSFORM

Wavelets are basis functions which are localized in both physical space (due to their finite support) and wave number space (e.g., Fig. 1). For comparison, the classical Fourier transform is based on functions (sines and cosines) that are well localized in frequency but do not provide localization in physical space due to their global support. Because of this space/scale localization, the wavelet transform provides both spatial and scale (frequency) information while the Fourier transform on the other hand only provides frequency information.

A field $u(\mathbf{x})$ can be represented in terms of wavelet basis functions as

$$u(\mathbf{x})=\sum_{\mathbf{l}\in\mathcal{L}^0} c_{\mathbf{l}}^0\phi_{\mathbf{l}}^0(\mathbf{x})+\sum_{j=0}^{+\infty}\sum_{\mu}\sum_{\mathbf{k}\in\mathcal{K}^{\mu,j}} d_{\mathbf{k}}^{\mu,j}\psi_{\mathbf{k}}^{\mu,j}(\mathbf{x}), \qquad (4)$$

where $\phi_{\mathbf{k}}^0(\mathbf{x})$ and $\psi_{\mathbf{l}}^{\mu,j}$ are, respectively, n-dimensional scaling functions and wavelets of different families (μ) and levels of resolution (j). Scaling function coefficients represent the averaged values of the field while the wavelet coefficients represent the details of the field at different scales. The wavelet functions have a zero mean while the scaling functions do not. Note that due to the local support of both scaling functions and wavelets, there is a one-to-one correspondence between the location of each scaling function or wavelet with a grid point. As a result each scaling function coefficient $c_{\mathbf{l}}^0$ and each wavelet coefficient $d_{\mathbf{k}}^{\mu,j}$ is uniquely associated with a single grid point by the indices $\mathbf{l}$ and $\mathbf{k}$, respectively.

Although the wavelet transform with its space/scale localization is an attractive technique to apply to the solution of problems with localized structures such as the simulation of turbulent flows, first generation wavelet transforms[27,28] have difficulties dealing with boundaries. Traditionally, one-dimensional first generation wavelets ψ_k^j are defined as translates and dilates of one basic wavelet ψ, i.e., $\psi_k^j(x)=\psi(2^jx-k)$. As a result, first generation wavelets are defined either on infinite or periodic domains.

Second generation wavelets[21,22] are a generalization of first generation wavelets that supplies the necessary freedom to deal with complex geometries, arbitrary boundary conditions, and irregular sampling intervals. Second generation wavelets form a Reisz basis for some function space, with the wavelets being local in both space and frequency and often having many vanishing polynomial moments, but without the translation and dilation invariance of their first generation cousins. Despite the loss of these two fundamental properties of wavelet bases, second generation wavelets retain many of the useful features of first generation wavelets, including a fast $O(N)$ transform.

The primary advantages of second generation wavelets over their first generation counterparts for this work are that they are constructed in the spatial domain and can be custom designed for complex multidimensional domains and irregular sampling intervals. The second generation wavelet transform is also a factor of 2 faster than the first generation wavelet transform. The construction of second generation wavelets is based on the lifting scheme that is discussed in detail by Sweldens.[21,22]

For this study we use a set of second generation wavelets known in the literature as lifted interpolating wavelets.[21,23] In particular, *a priori* tests are done using the lifted interpolating wavelet of order 6, hereafter referred to as LI6. The LI6

wavelet and its Fourier transform are shown in Fig. 1. For a more in-depth discussion on the construction of these wavelets the reader is referred to the papers by Sweldens[21,22] and Vasilyev and Bowman.[23] For a more general discussion on wavelets we refer to the books of Daubechies[29] and Mallat.[30]

III. WAVELET FILTERS

This section briefly describes the theory of wavelet filtering. The wavelet filter will be introduced by way of comparison with the more widely used Fourier cutoff filter. The Fourier cutoff filtering operation is performed by first transforming a field into Fourier space and then zeroing out the wave numbers that are greater than an *a priori* defined cutoff wave number. When the truncated modes are transformed back to real space, the filtered field is obtained. This operation is defined as

$$\overline{u}(\mathbf{x}) = (2\pi)^{-3/2} \sum_{\|\mathbf{k}\| \leqslant k_{\text{cutoff}}} \hat{\mathbf{u}}(\mathbf{k}) e^{i\mathbf{kx}}. \tag{5}$$

As discussed above the basis functions used (sines and cosines) in the Fourier transform have infinite support in real space and there is a one-to-one correspondence between Fourier modes and wave numbers (frequency space). To facilitate comparison with the wavelet filter, the Fourier cutoff filter can be viewed as first making a Fourier filter mask and then applying it to the Fourier space representation of the field to zero out the Fourier modes that are greater than the cutoff wave number. If we define a Fourier filter mask this way it will be constant for any field that the filter is applied to for a given constant cutoff mode k_{cutoff}. Because of the infinite support of the Fourier basis functions in real space there is no direct correspondence between the Fourier filter mask and the actual grid that is needed to support the filtered field in real space. Another important property of the Fourier filtered field is that it contains only frequencies represented by the modes below the cutoff wave number and the energy of these resolved frequencies will be unchanged by the Fourier filtering process. When applying a Gaussian filter, or any other filter that is coupled with an explicit Fourier cutoff filter, all these properties apply except the energy in the resolved frequencies will be modified by the filtering process.

Figure 2 shows the energy spectra of a turbulent field and the energy spectra of each of its Fourier modes (vertical lines). This turbulent field was obtained from a 256^3 DNS simulation of forced isotropic turbulence[12] with $\text{Re}_\lambda = 168$ and will hereafter be referred to as F_{256}. We can see how each Fourier mode is contained within a single frequency.

Wavelet filtering is performed in wavelet space using wavelet coefficient thresholding, which can be considered as a nonlinear filter that depends on each flow realization. For example wavelet filtering of the vorticity field is achieved by performing the following three steps:

(1) Perform the forward wavelet transform of $\boldsymbol{\omega}$;
(2) Set to zero those wavelet coefficients, whose magnitude is below an *a priori* prescribed threshold ϵ, i.e., $\|\tilde{\boldsymbol{\omega}}\|_2 \leqslant \epsilon$, where $\tilde{\boldsymbol{\omega}}$ is the wavelet transform of $\boldsymbol{\omega}$;
(3) Apply the inverse wavelet transform.

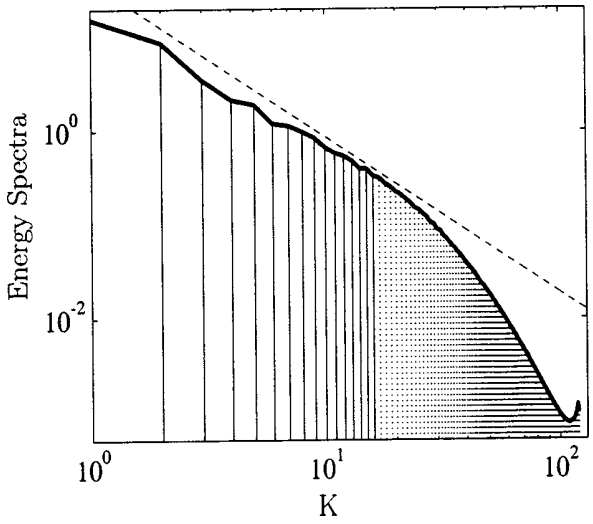

FIG. 2. Energy spectra of turbulent velocity field F_{256}: (—). Resolved Fourier modes less than or equal to cutoff wave number ($K_c = 16$): —. Residual Fourier modes greater than cutoff wave number: $(\cdots)$.

We will present below examples of applying the wavelet filter to the vorticity as well as the velocity field.

The wavelet thresholding filter is defined by

$$u_{\geqslant}(\mathbf{x}) = \sum_{\mathbf{l} \in \mathcal{L}^0} c_{\mathbf{l}}^0 \phi_{\mathbf{l}}^0(\mathbf{x}) + \sum_{j=0}^{+\infty} \sum_{\mu} \sum_{\substack{\mathbf{k} \in \mathcal{K}^{\mu,j} \\ |d_{\mathbf{k}}^{\mu,j}| \geqslant \epsilon}} d_{\mathbf{k}}^{\mu,j} \psi_{\mathbf{k}}^{\mu,j}(\mathbf{x}). \tag{6}$$

The reconstruction error due to wavelet filtering with threshold ϵ can be shown to be[24,31]

$$\|u(\mathbf{x}) - u_{\geqslant}(\mathbf{x})\| \leqslant C\epsilon, \tag{7}$$

where C is of order unity.

We can define a wavelet filter mask such that when applied in wavelet space, the wavelet coefficients greater than ϵ (under some norm) are set to zero. This wavelet filter mask is similar to what is earlier defined for the Fourier cutoff filter, except the wavelet filter mask, with constant ϵ, will be different for each field the wavelet filter is applied to. Another difference is that with the wavelet filter mask there is a one-to-one correspondence between the wavelet filter mask points and the grid points in real space. Here we see an important property of the wavelet thresholding filter: the grid required to support the wavelet filtered field will be changing in time and it will be collocated with the wavelet filter mask. Thus, the grid defined by the wavelet collocation points will track the areas of locally significant energy in physical space. Yet again nothing in the physical world "comes for free." Unlike the Fourier filter modes, there is no longer a one-to-one correspondence between wave number and wavelet level. Instead each wavelet level represents a region of wave numbers. A comparison of the important properties of the Fourier cutoff and wavelet thresholding filters is provided in Table I.

Figure 3 shows the energy spectra of the turbulent field F_{256} along with the energy spectra of six wavelet scales or levels. It should be noted that each wavelet scale has energy in a region of wave numbers and that these regions, associ-

TABLE I. Comparison of Fourier cutoff and wavelet thresholding filter properties.

Fourier cutoff filter	Wavelet thresholding filter
Bases with infinite support in space	Wavelet bases with local support in space and frequency
One-to-one correspondence in frequency	Wavelet level corresponds to a region of wave numbers
Approximately same number of points in Fourier mask and real space minimum support grid	One-to-one correspondence between wavelet mask and real space minimum support grid
No frequencies greater than cutoff wave number in filtered field	Filtered field can contain all frequencies
Filter mask is constant over all fields	Filter mask is specific to a field and tracks regions of high energy

ated with each wavelet scale, overlap. Figure 4 shows the energy spectra of the field F_{256} along with the filtered and residual fields resulting from the application of a wavelet thresholding filter. It can be seen that unlike the Fourier filtered field the wavelet filtered field contains energy at all wave numbers up to the Nyquist frequency.

IV. COHERENT VORTEX SIMULATION

A relatively new method for simulating turbulence, that uses the wavelet thresholding filter, called coherent vortex simulation, was recently introduced by Farge *et al.*[20] In a coherent vortex simulation (CVS) the vorticity field is decomposed into two parts using a wavelet thresholding filter:

$$\boldsymbol{\omega}=\boldsymbol{\omega}_{>}+\boldsymbol{\omega}_{\leqslant}, \tag{8}$$

where $\boldsymbol{\omega}_{>}$ is the filtered part of the flow defined on an adaptive grid and $\boldsymbol{\omega}_{\leqslant}$ is the SGS field that is made as close to Gaussian white noise as possible. It is important to note that the SGS field that results from the application of a wavelet filter can have energy in all frequencies represented in the original field [e.g., Fig. 4] and that this spectral content will vary with time and over the domain of the field. This contrasts with the SGS field in the LES of a homogeneous flow that contains no spectral content above the Fourier cutoff mode at any time.

The formulation for CVS then begins with the vorticity-transport equation:

$$\frac{\partial\boldsymbol{\omega}}{\partial t}=-(\mathbf{V}\cdot\nabla)\boldsymbol{\omega}+(\boldsymbol{\omega}\cdot\nabla)\mathbf{V}+\nu\nabla^2\boldsymbol{\omega}. \tag{9}$$

As in LES, after application of the wavelet filter we obtain the following CVS equation that describes the evolution of the filtered field:

$$\frac{\partial\boldsymbol{\omega}_{>}}{\partial t}=-(\mathbf{V}_{>}\cdot\nabla)\boldsymbol{\omega}_{>}+(\boldsymbol{\omega}_{>}\cdot\nabla)\mathbf{V}_{>}+\nu\nabla^2\boldsymbol{\omega}_{>}-\mathbf{f}, \tag{10}$$

where

$$\mathbf{f}=[(\mathbf{V}\cdot\nabla)\boldsymbol{\omega}]_{>}-[(\boldsymbol{\omega}\cdot\nabla)\mathbf{V}]_{>} -(\mathbf{V}_{>}\cdot\nabla)\boldsymbol{\omega}_{>}+(\boldsymbol{\omega}_{>}\cdot\nabla)\mathbf{V}_{>} \tag{11}$$

is the SGS forcing that needs to be modeled. The localized nature of the SGS forcing will have to be considered in defining SGS stress models for use with CVS.

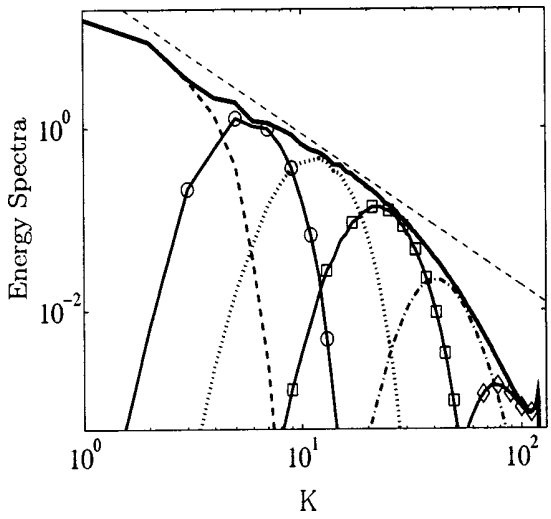

FIG. 3. Energy spectra of turbulent velocity field F_{256}: (—), contained in wavelet levels. Level 1: (– – –), Level 2: (—○—), Level 3: (···), Level 4: (—□—), Level 5: (—·—), Level 6: (—◇—).

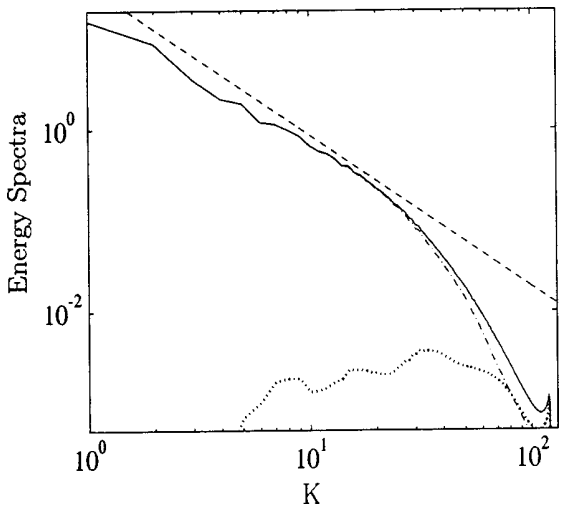

FIG. 4. Velocity wavelet filtering applied to DNS of forced homogeneous turbulence (field: F_{256}) at ϵ_{opt}. DNS field (——). Filtered field using LI6 wavelets (95% compression): (—·—), residual field: (···). The wavelet compression is defined as $(N-N_{>})/N\times 100\%$, where $N_{>}$ is the number of retained wavelet coefficients for a given threshold ϵ.

It has been shown that, when a nonlinear wavelet thresholding filter is applied to a moderately high Reynolds number isotropic turbulent vorticity field, the residual field is closer to being statistically Gaussian than when a Fourier cutoff filter with the same number of modes is used.[14,15,20,32,33] Thus, it is expected that with wavelet filtering the SGS stress can be modeled more accurately than with Fourier filtering. This has not been proven and is a current topic of research. Coherent/incoherent decomposition has been shown in Refs. 20, 32, and 33 in two dimensions and will be shown in Sec. V below in three dimensions. The decomposition of turbulent three dimensional fields is also shown in Refs. 14 and 15.

In CVS the optimal value of ϵ must be found at each time step such that the wavelet filter decomposes the vorticity field into a filtered field that contains all the coherent vortices of significant energy and a SGS field that is as close to Gaussian white noise as possible. In Ref. 20 the optimal value for ϵ is found using Donoho's denoising procedure[34] which can be described as follows: given a function that is the superposition of a smooth function and Gaussian white noise, one performs a forward wavelet transform, and sets to zero the "noisy" wavelet coefficients if the square of the wavelet coefficient is less than the noise variance σ^2. This procedure, known as hard or linear thresholding, is optimal for denoising signals in the presence of Gaussian white noise because wavelet-based estimators minimize the maximal L^2-error for functions with inhomogeneous regularity. Since the variance of the Gaussian white noise component of a turbulence field is not a known quantity, Farge *et al.*[20] proposed to base the wavelet threshold ϵ on the variance of the full field instead.

V. WAVELET FILTERING OF TURBULENT FLOWS

As we discussed in Sec. IV it has been established[14,15] that a first generation orthogonal wavelet filter can be used to decompose a turbulent vorticity field into a coherent non-Gaussian part and an incoherent Gaussian part. We will show in this section that a second generation bi-orthogonal wavelet filter is also able to accomplish this coherent/incoherent decomposition. In addition we will show that the second generation wavelet filter is capable of decomposing a velocity field into coherent and incoherent subfields. This is of particular interest in studying different eddy capturing methods because it allows us to directly calculate the SGS dissipation after applying the wavelet filter.

To demonstrate the ability of the second generation wavelet filter to decompose an isotropic turbulence vorticity and velocity field we will consider the L_∞-error (scaled by the standard deviation) between the probability density function (PDF) of the subgrid field and a Gaussian PDF with the same mean and variance, which is defined by

$$E_\infty = \sigma \| \mathrm{PDF}(\mathbf{u}_\leqslant) - \mathrm{PDF}_{\mathrm{Gauss}}(\mathbf{u}_\leqslant) \|_\infty . \tag{12}$$

In Fig. 5 three different filters at varying compression are applied to the isotropic turbulence field F_{256}. We define the compression as $(N-N_>)/N \times 100\%$, where $N_>$ is the number of retained wavelet coefficients for a given threshold ϵ.

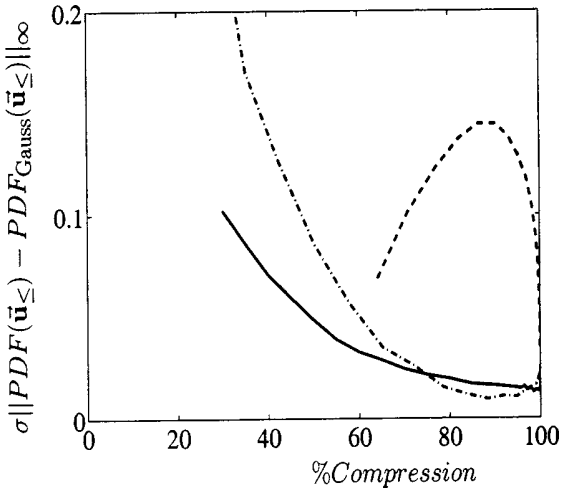

FIG. 5. Normalized L_∞-error between the SGS field and Gaussian PDFs with the same mean and variance. Wavelet filter applied to: velocity (——), vorticity (–·–), Fourier filter (– – –).

In the case of the Fourier cutoff filter $N_>$ is the number of retained Fourier coefficients for a given cutoff wave number K_c. With this notation 0% compression results in the full DNS field and 100% compression results in an empty resolved field. The first two filters used are the second generation LI6 wavelet filter applied to the vorticity field and the LI6 wavelet filter applied to the velocity field. The third filter is a Fourier cutoff filter applied to the velocity field. We note that a Fourier cutoff filter commutes with differentiation, so application of the Fourier cutoff filter to the velocity or vorticity field will give the same results. The wavelet filtering is implemented as defined in Sec. III. For this study we projected the filtered field into divergence free space after the wavelet filtering operation. This is necessary because the wavelet basis used are not divergence free. The use of a divergence free projection with the wavelet filter is discussed further in Appendix B. The filter widths were varied to achieve a range of compression from 30% to 99.996948% for each of the filters. The maximum compression corresponds to $K_c = 8$ for the Fourier filter (8^3 modes) or 8^3 pure scaling functions for the wavelet filter. In these tests all the 8^3 wavelet scaling functions are always retained [see Eq. (4)].

We can see in Fig. 5 that for the wavelet filter applied to the velocity or vorticity fields there exists a compression where the scaled L_∞-error (E_∞) is minimized. For vorticity filtering this minimum occurs at a compression of 90%, whereas for velocity filtering this minimum occurs at a higher compression of 99.5%. Using a Fourier filter results in an error trace that is concave downward with the minimum occurring at the highest compression ($K_c = 8$). In comparison, for the full DNS velocity field $E_\infty = 0.47$. We also see in Fig. 5 that E_∞ for all three filters converge as they get to the maximum compression of $K_c = 8$ for the Fourier filter (8^3 modes) or 8^3 pure scaling functions for the wavelet filter. This convergence is because a wavelet filter with only scaling functions retained is close to a sharp cutoff Fourier filter.[35,36]

In the work done by Farge *et al.*[20] an optimal compres-

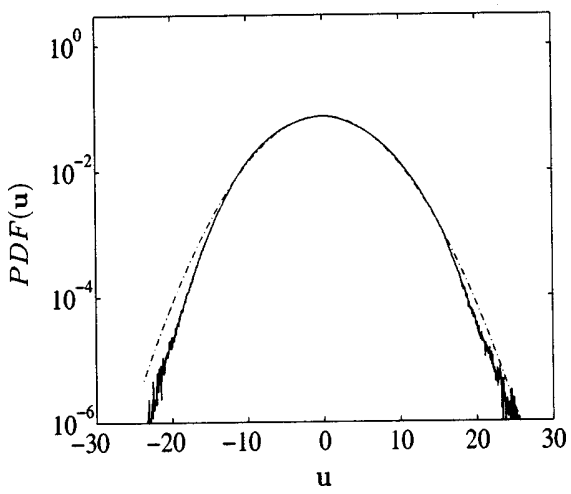

FIG. 6. PDF of forced isotropic turbulence velocity field F_{256}: (——). Gaussian PDF with same mean and variance: (—·—).

sion is defined such that the subgrid field is statistically close to Gaussian white noise. Thus, the resolved field is presumed to be more coherent, since the incoherent modes have been removed. We will define the optimal Gaussianity compression (OGC) as the compression that minimizes the scaled L_∞-error, E_∞ [see Eq. (12)]. For the wavelet filter applied to the vorticity field the OGC is 90.0% and for the wavelet filter applied to the velocity field the OGC is 99.5%.

It is also of interest to directly compare the PDF of the residual velocity field at the OGC for the velocity and vorticity applied wavelet filters and the Fourier cutoff filter with the same compression ratio. First, for reference, the PDF of the full velocity field is shown in Fig. 6. Figure 7(a) shows the PDF of the residual and resolved velocity field after applying the wavelet filter to the velocity DNS field at the optimal Gaussianity compression of 99.5%. Figure 7(b) shows the PDF of the residual and resolved velocity field after applying a Fourier cutoff filter with the same compression ratio. It can be seen from these figures that the residual PDF is close to Gaussian for the wavelet filter. In the case of the Fourier filter the PDF of the residual field deviates significantly from the Gaussian PDF in the tails. The residual, when the wavelet filter is applied to the velocity field, is clearly more Gaussian than the residual from the Fourier cutoff filter. We see in Fig. 8 that this is also the case when the wavelet filter is applied to the vorticity field.

The results of this study and previous work[13–15,20,32,33] clearly demonstrate that the vorticity wavelet filter is able to decompose an isotropic turbulence field into a coherent, non-Gaussian part and a incoherent, ''near'' Gaussian part. Here we have added the result that a velocity wavelet filter is able to decompose an isotropic turbulence field in the same way.

The real advantage of applying the wavelet filter to the velocity field is that it allows us to directly calculate the SGS dissipation $(-\tau_{ij}\overline{S}_{ij})$, where $\overline{S}_{ij}=\overline{S}_{ij}^{>\epsilon^{\mathcal{P}}}$ for the wavelet filter [see Eq. (B9)] and $(\,)^{\mathcal{P}}$ is a divergence free projection operator defined in Appendix B [see Eq. (B1)]. Figure 9(a) shows the total subgrid scale dissipation normalized by the DNS viscous stress dissipation for the wavelet and Fourier filter applied to the velocity field. Both filters produce a total subgrid scale dissipation that increases with compression. Yet with the wavelet filter the total subgrid scale dissipation stays flat relatively longer than with the Fourier filter. This difference shows the possible advantaged of using a wavelet filter. For a given compression ratio, the subgrid scale dissipation that will have to be modeled when a wavelet filter is used will be less than when a Fourier filter is used. To quantify this difference, Fig. 9(b) shows the percent difference between the total subgrid scale dissipation with the wavelet and the Fourier filters. We see that the largest difference is at 70% compression where the wavelet filter results in a SGS dissipation 70% lower in comparison to using the Fourier cutoff filter. In the region of compression that is of more interest for actual simulations we see that the difference is still significant. At 95% compression the difference using the wavelet filter is still 50%. We anticipate an even higher difference for high Reynolds number turbulent flows. This

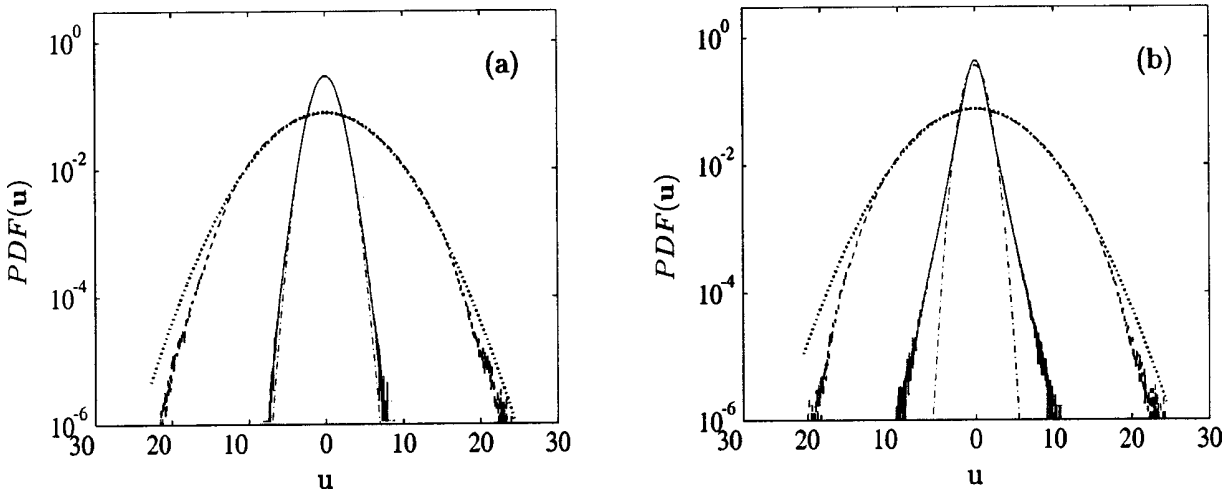

FIG. 7. PDF of forced isotropic turbulence velocity field F_{256} using (a) LI6 wavelet filter applied to the velocity at 99.5% compression and (b) Fourier cutoff filter at the equivalent compression. Filtered field: (– – –), with its associated Gaussian: (···). SGS field: (——), with its associated Gaussian: (—·—).

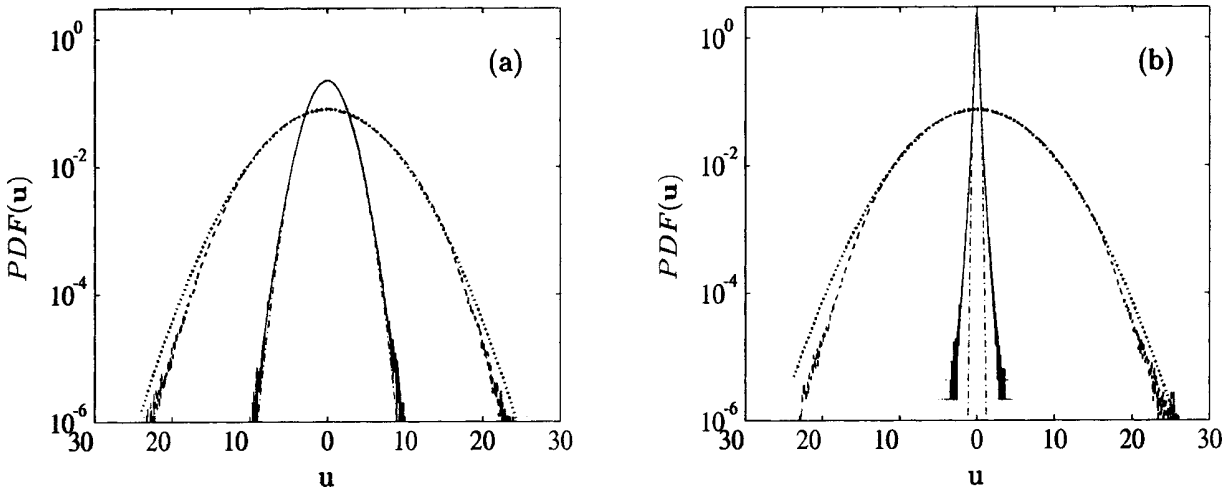

FIG. 8. PDF of forced isotropic turbulence velocity field F_{256} using (a) LI6 wavelet filter applied to the vorticity at 90.0% compression and (b) Fourier cutoff filter at the equivalent compression. Filtered field: (– – –), with its associated Gaussian: (· · ·). SGS field: (——), with its associated Gaussian: (—·—).

highlights a possible advantage of using a wavelet filter in an eddy capturing method. The wavelet filter decomposes the turbulent field such that there is significantly less SGS dissipation that has to be modeled.

To understand the physical reasons why the SGS dissipation varies between the use of the wavelet and the Fourier filter we can compare the average correlation between the components of τ_{ij} and S_{ij} for the two filters. In Fig. 10 we see that, like the SGS dissipation, the correlation using the wavelet filter stays flat relatively longer than with the Fourier filter. If we compare Figs. 9(a) and 10 we see that for both filters the total SGS dissipation increases as the correlation between τ_{ij} and S_{ij} increases. The lower SGS dissipation for the wavelet filter follows the trend of the lower correlation between τ_{ij} and S_{ij}. From these plots it can be seen that the lower SGS dissipation for the wavelet filter is due to the lower correlation between τ_{ij} and S_{ij} which is caused by the SGS field being relatively more incoherent.

Another way to define the optimal wavelet filter threshold for coherent and incoherent field decomposition is to base it on the SGS dissipation. In terms of the wavelet based methods discussed in this work the ideal resolved field is the one that minimizes the SGS dissipation due to the SGS modes. Unfortunately the SGS dissipation does not have a minimum (see Fig. 9), so an additional constraint must be added in order to maximize the field compression at the same time. Based on this combined criteria the optimal wavelet threshold (ϵ_{opt}) can be defined. This definition results in an optimal field compression of 95% in the case of the isotropic turbulence field F_{256} using the LI6 wavelet filter applied to the velocity field. From here on we will refer to the wavelet filter threshold ϵ that results in the "optimal" wavelet compression as ϵ_{opt} and the resolved and residual fields defined by wavelet filtering at ϵ_{opt} as the "coherent" and "incoherent" fields. Note that our definition of coherent structures is very different from other known definitions.[37,38]

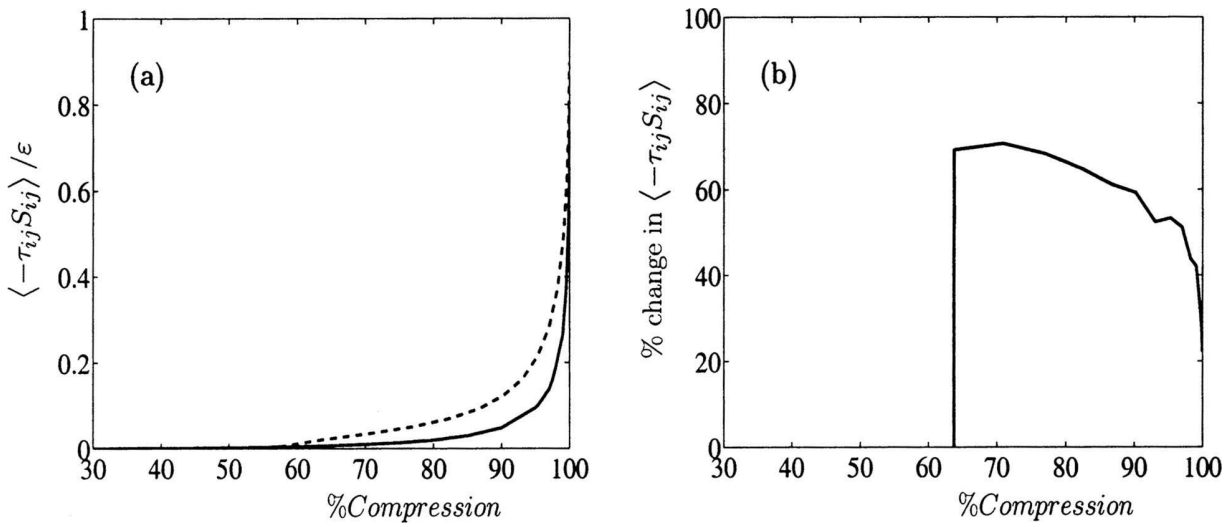

FIG. 9. (a) Mean subgrid scale dissipation normalized by the full field mean viscous dissipation, $\epsilon=\langle 2\nu S_{ij}S_{ij}\rangle$. Wavelet filter applied to: velocity (——). Fourier filter (– – –). (b) % difference in mean subgrid scale dissipation between wavelet filtering and Fourier filtering.

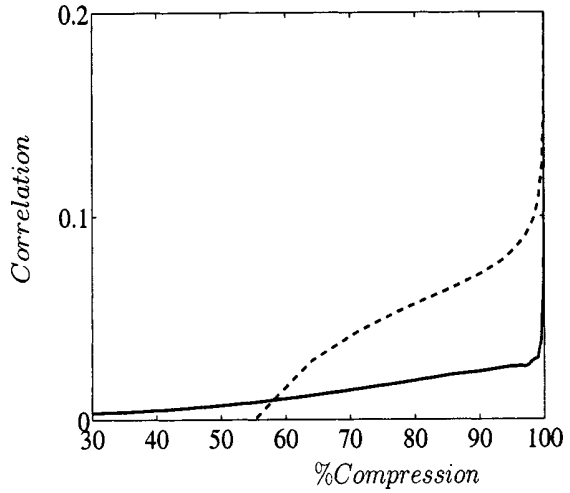

FIG. 10. Correlation between τ_{ij} and S_{ij}. Wavelet filter applied to: velocity (——). Fourier filter (– – –).

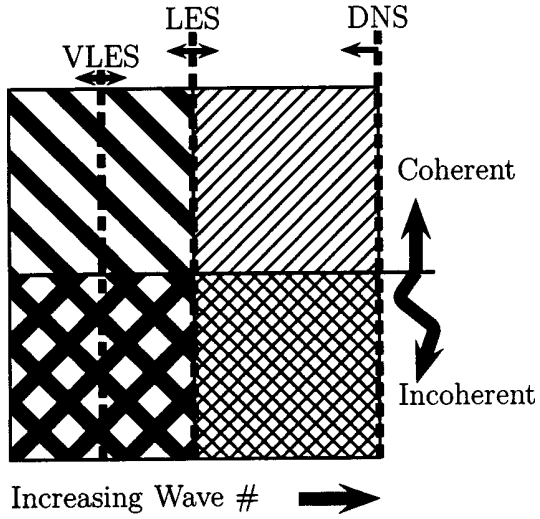

FIG. 12. Coherency diagram of the turbulent field for DNS, VLES, and LES.

VI. COHERENCY DIAGRAM OF A TURBULENT FIELD

A key part of this work has been to understand different filter types and their effect on the physical interaction between the residual and filtered fields in large eddy capturing methods such as LES and CVS. To do this, we introduce a coherency diagram of a turbulent field in terms of wave number and wavelet threshold ϵ (see Fig. 11). In this figure a vertical line can be thought of as dividing the field into resolved (below the cutoff wave number) and residual (above the cutoff wave number) fields. This is, of course, the result of explicitly applying a Fourier cutoff filter to the field. It is also the result of representing the field on a reduced regular grid, thus implicitly filtering the field. Now the same field can be separated by applying a wavelet thresholding filter. In Fig. 11 this is represented by drawing a horizontal line across the square at a given wavelet filter threshold of ϵ. As discussed earlier there exists some "optimal" ϵ such that the square can be divided into coherent and incoherent parts. Now from this coherency diagram it can be immediately inferred that when the field is separated using a Fourier cutoff filter the resulting subgrid contains both coherent and incoherent parts. This result will be explored further below.

In Fig. 12 the vertical lines of separation on the coherency diagram for DNS, LES, and VLES are shown. First it is clear that in DNS there is no subgrid by definition so the separation line is at the highest wave number needed to capture the physics of the turbulent field down to the Kolmogorov scale. Then the vertical line for LES is shown that divides the field at some Fourier cutoff wave number, usually taken to be in the inertial range. At an even lower wave number we have the vertical separation line for very large eddy simulation. Figure 13 shows the energy spectra of DNS field F_{256}. The energy spectra after a LES and a VLES Fourier cutoff filter is applied are also shown.

In the next two sections we will introduce two new methodologies that have come out of our work to build a

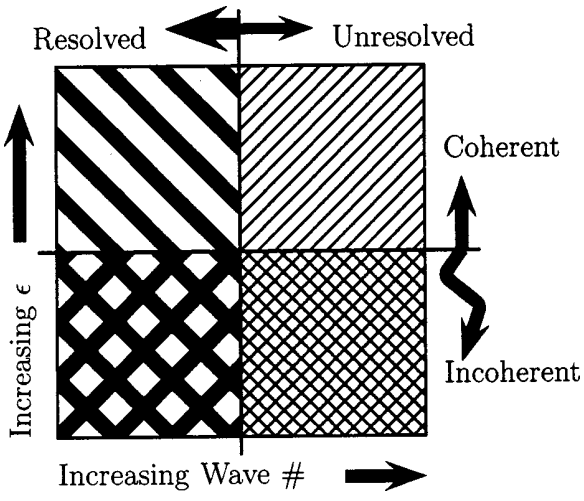

FIG. 11. Coherency diagram of the turbulent field.

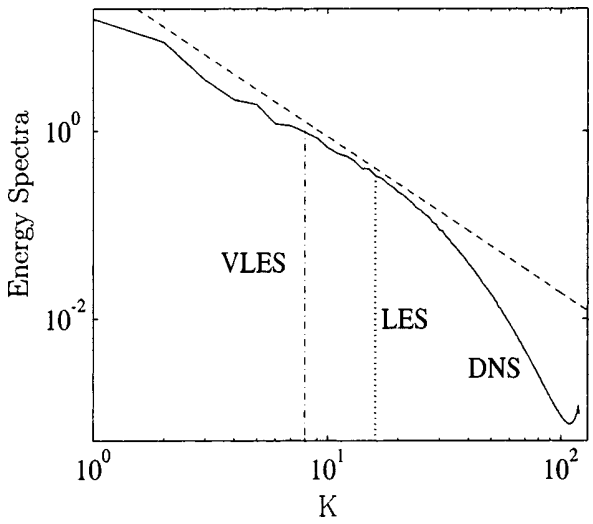

FIG. 13. DNS field (——), VLES filtered field (—·—), and LES filtered field (···).

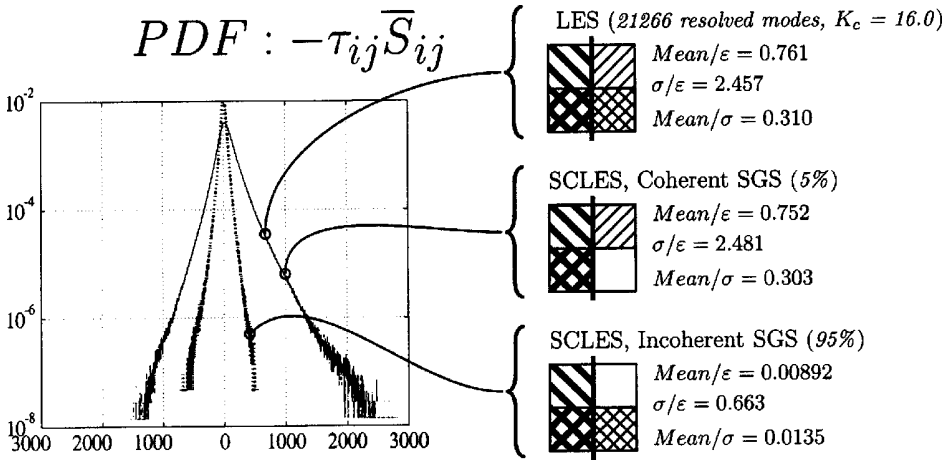

FIG. 14. SCLES subgrid scale dissipation for homogeneous turbulence field F_{256}. Fourier cutoff filter ($K_c=16$) is used along with a velocity field wavelet filter using LI6 wavelets.

theoretical framework to understand the relationship between CVS and LES in terms of the coherency diagram presented above. In Sec. VII we will introduce the stochastic coherent large eddy simulation method that is based on the fact that the LES subgrid contains both coherent and incoherent parts as discussed above. Then in Sec. VIII the stochastic coherent adaptive large eddy simulation method will be introduced as an integration of the ideas of LES and CVS that in computational cost will be similar to LES.

VII. STOCHASTIC COHERENT LARGE EDDY SIMULATION

Stochastic coherent large eddy simulation (SCLES) is a different way to look at LES. In current LES implementations there is no clear distinction made between modeling the SGS dissipation due to the coherent vs the incoherent SGS modes. In this section we will present *a priori* tests showing that in nonadaptive LES with a Fourier cutoff filter the majority of the SGS dissipation is due to a small percentage of coherent modes in the subgrid scales. Given this result we propose the SCLES methodology in which the SGS stress due to the coherent and the incoherent SGS modes is modeled separately.

When developing LES subgrid scale models the assumption is usually made that the filtering operation separates the large eddies from the smaller ones and that the resulting residual subgrid scales being modeled have a generally universal character.[17,18] Yet in the coherency diagram discussed above (see Figs. 11 and 12) it is clear that the LES subgrid scales contain coherent structures in an incoherent background.

In evaluating the SCLES approach the quantity of particular interest is the SGS dissipation due to the coherent vs the incoherent modes in the subgrid scales. For the convenience of discussion we will hereafter refer to the SGS dissipation due to the coherent and the incoherent SGS modes, respectively, as the coherent and incoherent SGS dissipation. The coherent and incoherent SGS dissipation can be found by first decomposing the subgrid scale stress (τ_{ij}) [Eq. (3)] into the contributions from the coherent and incoherent parts of the subgrid scale modes. To accomplish this we first decompose the subgrid scale field $u_i' \equiv u_i - \overline{u_i}$ into its coherent and incoherent parts

$$u_i' \equiv u_i'^{(C)} + u_i'^{(I)} = (u_{>\epsilon\mathrm{opt}})' + (u_{<\epsilon\mathrm{opt}})'.$$

The SGS stress (τ_{ij}) can then be defined as

$$\tau_{ij} = \tau_{ij}^{(C)} + \tau_{ij}^{(I)}, \tag{13}$$

where

$$\tau_{ij}^{(C)} = \overline{\overline{u_i} u_j'^{(C)} + \overline{u_j} u_i'^{(C)}} + \overline{u_i'^{(C)} u_j'^{(C)}}, \tag{14}$$

and

$$\tau_{ij}^{(I)} = \overline{\overline{u_i} u_j'^{(I)} + \overline{u_j} u_i'^{(I)}} + \overline{u_i'^{(I)} u_j'^{(I)}} + \overline{u_i'^{(C)} u_j'^{(I)} + u_j'^{(C)} u_i'^{(I)}}. \tag{15}$$

The SGS dissipation due to the coherent and incoherent SGS modes is then defined as

$$-\tau_{ij}\overline{S}_{ij} = -\tau_{ij}^{(C)}\overline{S}_{ij} - \tau_{ij}^{(I)}\overline{S}_{ij}. \tag{16}$$

In Fig. 14 we present the probability density function (PDF) of the SGS dissipation due to the full SGS stress after the application of a Fourier cutoff filter ($K_c=16$), along with the coherent and the incoherent SGS dissipation. Backscatter on the PDF plot is in the negative direction on the horizontal axis. We emphasize that in SCLES the PDF of the full and the coherent SGS dissipation are nearly identical, even though the coherent SGS contains only 5% of the modes of the original subgrid field. In both cases it can be seen that the mean of the PDF is positive. This shows that there is both forward and backscatter, but the net SGS dissipation is positive. The incoherent SGS dissipation has a lower standard deviation and is characterized by a PDF that is nearly symmetrical around zero. As an indicator of the contribution to the total SGS dissipation we calculate the mean SGS dissipation normalized by the mean viscous dissipation ($\epsilon = \nu\langle 2S_{ij}S_{ij}\rangle$) and the standard deviation (σ). The relative support of the PDF is characterized by the standard deviation

TABLE II. Comparison of SGS dissipation for LES, CVS, SCLES, and SCALES. ($\epsilon=\langle 2\nu S_{ij}S_{ij}\rangle$). We note that for the SCLES, 98.8% of the total SGS dissipation is due to the coherent part of the SGS field. While for SCALES, 99.5% of the total SGS dissipation is due to the coherent part of the SGS field.

	LES	SCLES	CVS	SCALES
% Compression	99.8732%($K_c=16$)	99.8732%	95.0%	99.8732%
% Optimal compression		95.0%	95.0%	95.0%
SGS dissipation				
Mean/ϵ	0.761	0.761	0.0947	0.552
σ/ϵ	2.457	2.457	1.795	4.700
Mean/σ	0.310	0.310	0.0527	0.118
Coherent SGS dissipation				
Mean/ϵ		0.752		0.549
σ/ϵ		2.481		4.709
Mean/σ		0.303		0.117
Incoherent SGS dissipation				
Mean/ϵ		0.00892		0.00321
σ/ϵ		0.663		0.390
Mean/σ		0.0135		0.00823

normalized by the mean viscous dissipation (σ/ϵ). These statistics are shown in Fig. 14 and are summarized in Table II for all the eddy capturing methods discussed in this paper. The spectral content of the coherent and incoherent SGS dissipation is shown in Fig. 15. The energy spectra of the full isotropic turbulence field used in these *a priori* tests, along with the resolved modes and the coherent and incoherent modes of the SGS field are shown in Fig. 16. From these statistics we can conclude that 98.8% of the total SGS dissipation is due to the 5% of the SGS modes that make up the coherent part of the SGS field.

The idea of the SCLES methodology is to model the effect of the coherent and incoherent parts of the SGS separately. An incoherent SGS model can make use of the near Gaussian statistics of the incoherent subgrid scales to model them stochastically. Given the relatively low amount of SGS dissipation due to the incoherent modes it maybe possible that an incoherent SGS model is not necessary. From the above *a priori* results we can see that the coherent SGS model should account for the majority of the SGS dissipation. In designing a coherent SGS model one would want to start by quantifying how the resolved scales and the coherent SGS modes are correlated. The fact that the coherent SGS dissipation accounts for such a large percent (98.8% in this example) of the SGS dissipation proves that the resolved scales and the coherent SGS modes are correlated to a high degree. Quantifying the physical relationships between the coherent structures in the resolved and unresolved fields is the subject of ongoing research. It is clear from this example (Fig. 17) that the effort to quantify these physical relation-

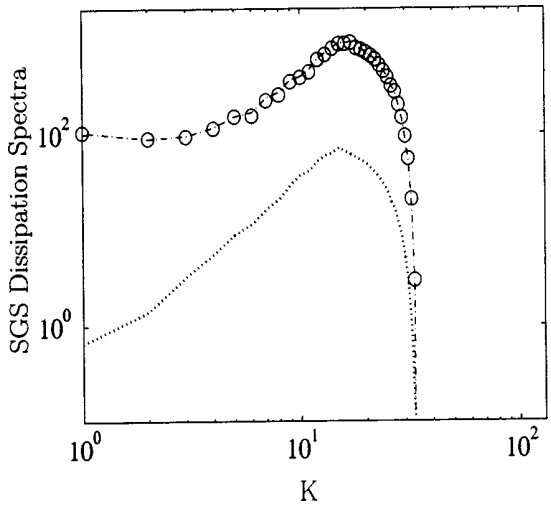

FIG. 15. SGS dissipation spectra ($-\tau_{ij}\bar{S}_{ij}$) after Fourier cutoff filtering at $K_c=16$ or a compression of 99.8732% (SCLES). Full SGS dissipation (○), coherent SGS dissipation: (—·—), incoherent SGS dissipation: (···).

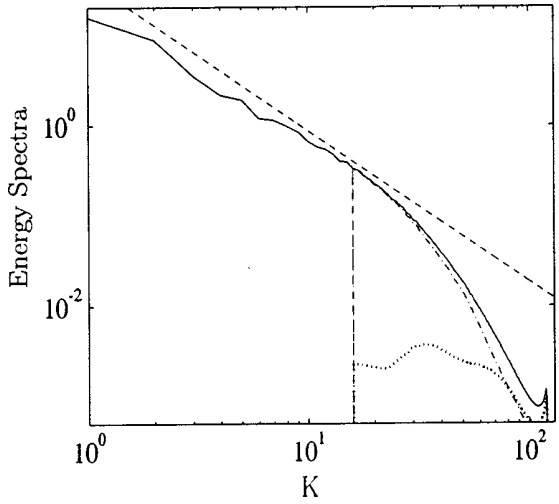

FIG. 16. DNS field (——), SCLES resolved field is same as DNS up to $K_c=16$ as in LES. Coherent part of subgrid field: $(u_{>\epsilon\mathrm{opt}})'$ (—·—). Incoherent part of subgrid field: $(u_{<\epsilon\mathrm{opt}})'$ (···).

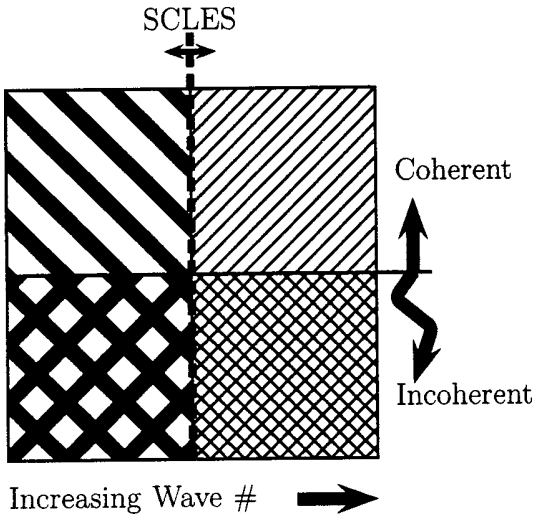

FIG. 17. Coherency diagram of turbulent field for SCLES.

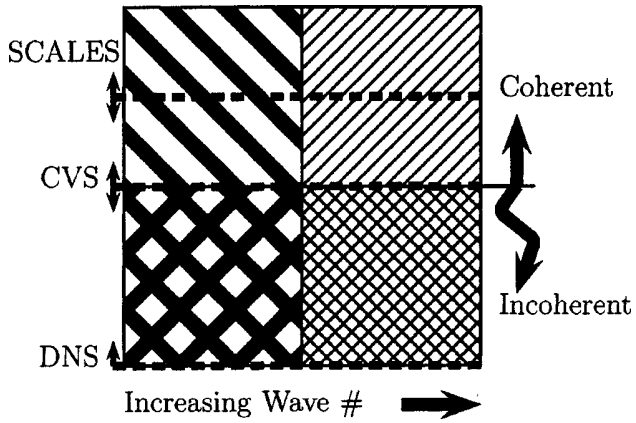

FIG. 18. Coherency diagram of turbulent field for DNS, CVS, and SCALES.

ships could benefit the LES community by providing the basis for more effective coherent structure based subgrid scale models.

The SCLES method retains the two major drawbacks of the classical LES method. First there is too much coherency in the SGS field and second is it not temporally adaptive which limits its use in the class of problems dominated by temporally changing physical characteristics. These drawbacks are addressed in the CVS approach but, as discussed above, the computational cost of CVS is believed to be prohibitive for high Reynolds number turbulent flows. In the next section we will introduce the stochastic coherent adaptive large eddy simulation method that attempts to combine the strengths of LES and CVS.

VIII. STOCHASTIC COHERENT ADAPTIVE LARGE EDDY SIMULATION

The SCALES methodology is based on applying a wavelet filter such that the maximum number of modes in each time step of a simulation are resolved in the simulation given the balance between computing resources and defined acceptable simulation error. Thus the most important modes are simulated given the resources available. The relationship between the SCALES methodology and other methods is best presented in terms of the coherency diagram of a turbulent field discussed in Sec. VI. In Fig. 18 the horizontal lines of separation on the coherency diagram for DNS, CVS, and SCALES are shown. The DNS line is at $\epsilon=0$ which is the same as no filter. The CVS line is where the field is ''optimally'' divided with the coherent structures in the resolved field and the incoherent residual in the subgrid field. The SCALES line is at a higher ϵ implying that for SCALES the resolved field is made up of coherent structures but the residual field is made up of both coherent and incoherent parts.

In this section we will perform *a priori* tests to show the nature of the coherent and incoherent modes in the residual field, and the coherent and incoherent SGS dissipation, using the SCALES methodology. We define SCALES wavelet filtering such that the number of resolved modes is approximately equivalent to an appropriate LES cutoff filter. For these *a priori* tests this would be $K_c=16$ or a field compression of 99.8732%. Note a spherical Fourier cutoff filter is used. Figure 4 shows the energy spectra of the field F_{256} of forced isotropic turbulence that has been wavelet filtered at ϵ_{opt} resulting in a compression of 95% for this field. Figure 19 shows the energy spectra of the same field F_{256} that has been wavelet filtered at the SCALES wavelet filter threshold of 99.8732%. It can be seen that in the case of wavelet filtering using ϵ_{opt} (Fig. 4) the energy spectra of the filtered field is virtually identical to the DNS energy spectra in the inertial range. It then falls off faster than the DNS data in the dissipative range but it still maintains the same character as the DNS energy spectra. The SCALES wavelet filtered field (Fig. 19) on the other hand falls off faster than the DNS data throughout the inertial range. Comparing the residual field trace in Figs. 4 and 19 it can be seen how increasing the wavelet filter threshold effects the spectral content of the residual field.

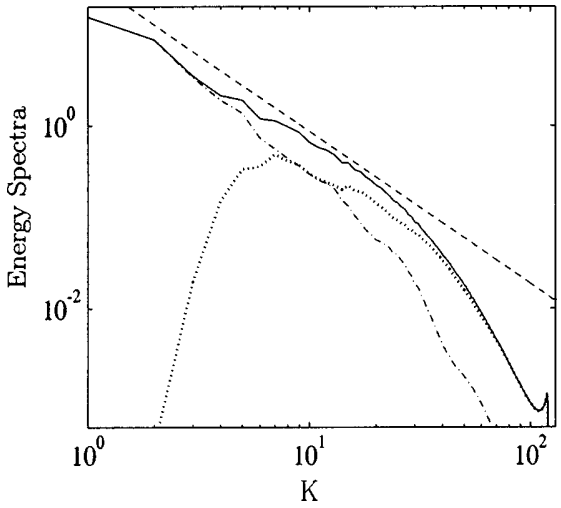

FIG. 19. DNS field (——) wavelet filtered at high ϵ (99.8732% compression) for SCALES using LI6 wavelets. Filtered field: (—·—), residual: (···).

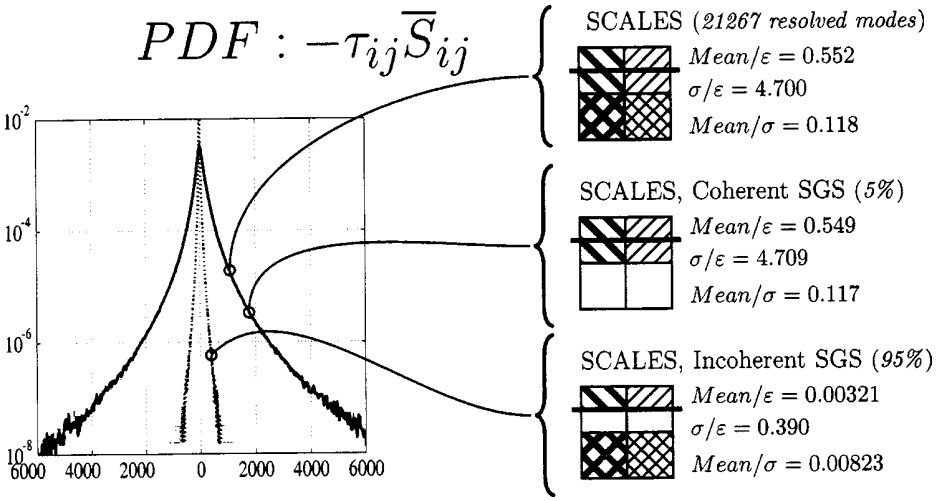

FIG. 20. SCALES subgrid scale dissipation for homogeneous turbulence field F_{256}. Wavelet filter using LI6 wavelets is used.

To calculate the SGS dissipation due to the coherent and incoherent modes, as we did with SCLES, we begin by decomposing the subgrid scale stress (τ_{ij}) [Eq. (3)] into the contributions from the coherent and incoherent parts of the subgrid scale modes. The subgrid scale field $u_{i<\epsilon\text{SCALES}} \equiv u_i - u_{i>\epsilon\text{SCALES}}$ can then be decomposed into its coherent and incoherent parts as

$$u_{i<\epsilon\text{SCALES}} \equiv u^{(C)}_{i<\epsilon\text{SCALES}} + u^{(I)}_{i<\epsilon\text{SCALES}} = (u_{>\epsilon\text{opt}})_{<\epsilon\text{SCALES}} + (u_{<\epsilon\text{opt}})_{<\epsilon\text{SCALES}}. \quad (17)$$

Then the equation for calculating the coherent and incoherent SCALES SGS dissipation is identical to the coherent and incoherent SCLES SGS dissipation [Eqs. (14) and (15)] if we redefine $\overline{(\ )}$ and $(\ )'$ as $\overline{(\ )} \equiv u_{>\epsilon\text{SCALES}}$ and $(\ )' \equiv u_{<\epsilon\text{SCALES}}$, respectively. The difference is that for these *a priori* tests, two wavelet filters are used, instead of a Fourier cutoff filter and a wavelet filter. Note that in an actual SCALES simulation only one wavelet filter is used.

In Fig. 20 we show the probability density function of the SGS dissipation ($-\tau_{ij}S_{ij}$) for the SGS field from a wavelet filter applied in the SCALES range to the DNS field F_{256}. Also shown are the coherent and incoherent SCALES SGS dissipation. By comparing the normalized means of the SGS dissipation in the three cases (along the right edge of Fig. 20 and summarized in Table II) we can see that 99.5% of the total SGS dissipation is due to 5% of the SGS modes that make up the coherent part of the SGS field. Figure 21 shows the energy spectra of the full, coherent and incoherent SGS dissipation. Comparing this figure with Fig. 15 highlights the different spectral content of the SGS dissipation between LES or SCLES (using a Fourier cutoff filter) and SCALES (using a wavelet filter).

The issues in developing SGS models for SCALES are the same as those discussed in Sec. VII for SCLES SGS models. Although in this work we have not explicitly shown the correlation between the resolved coherent modes and the unresolved coherent SGS modes, it is clear from the above results that they are correlated to a high degree. Quantifying the physical relationships between the coherent structures in the resolved and unresolved fields with SCALES filtering is the subject of ongoing research efforts. Since the large majority of the SGS dissipation in both SCLES and SCALES is due to the coherent modes in the subgrid scales, we anticipate that existing SGS models will perform adequately to represent the coherent SGS stress for initial testing of the SCALES method. However new models may show an improvement with the SCALES methodology. What is gained with SCALES over SCLES and LES, even using existing SGS models, is a method that is fully adaptive that "tracks" the energetic structures in the field.

Due to the adaptive nature of the SCALES method an adaptive wavelet collocation method[23–26] is ideally suited for its implementation. In the adaptive wavelet collocation method there is a one-to-one correspondence between grid points and wavelets, which makes calculation of nonlinear terms simple and allows the grid to adapt automatically and

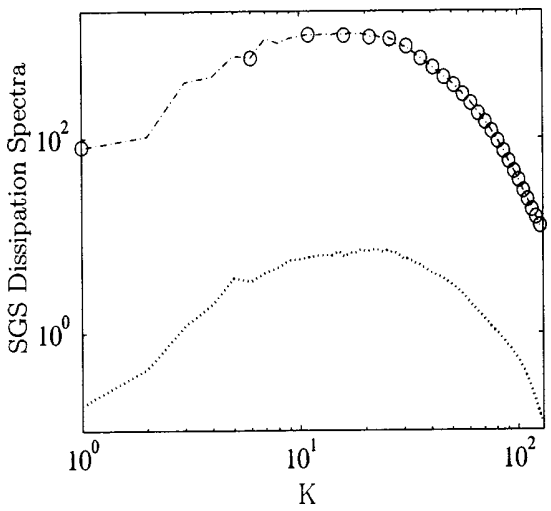

FIG. 21. SGS dissipation spectra ($-\tau_{ij}\overline{S}_{ij}$) after LI6 velocity wavelet filtering at a compression of 99.8732% (SCALES). Full SGS dissipation (○), coherent SGS dissipation: (—·—), incoherent SGS dissipation: (···).

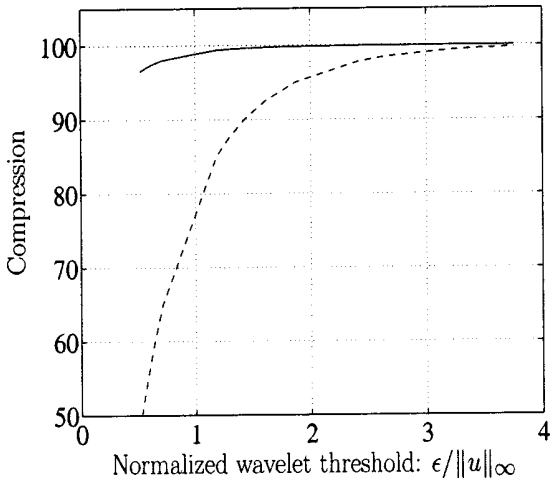

FIG. 22. Field compression vs normalized wavelet threshold $\epsilon/\|u\|_\infty$ using velocity wavelet filtering without adjacent zone (——) and with adjacent zone (– – –) for field F_{256}. It can be seen that as ϵ increases the loss in compression due to the adjacent zone becomes less significant.

dynamically to the solution by adding or removing wavelets. Very briefly, at each time step we take the wavelet transform of the solution, remove all wavelets with coefficient magnitude less than a threshold ϵ, and then reconstruct the solution. It can be shown that the L_∞ error of this approximation is $O(\epsilon)$. To account for the evolution of the solution over one time step we add the nearest neighbor wavelet coefficients in position and scale. While the cost of this added adjacent zone is significant at low compression ratios it becomes much less so at higher compression ratios. Figure 22 shows the compression ratio vs the wavelet filter threshold ϵ for a wavelet collocation grid with and without an adjacent zone. We can see clearly that the added overhead of the adjacent zone becomes insignificant for compression ratios over 98%. Since each wavelet corresponds to a single grid point this procedure allows the grid to automatically follow the evolution of the solution in position and scale. This method is based on second generation wavelets,[22] which allow the order of the wavelet (and hence of the numerical method) to be easily varied. The method has a computational complexity $O(N)$, where N is the number of wavelets retained in the calculation (i.e., those wavelets with coefficients greater than ϵ plus nearest neighbors). With this adaptation strategy a solution is obtained on a grid that ''tracks'' the coherent vortices in the field. An adaptive wavelet collocation solver is being developed in parallel to this work.[24,25] In Appendix A a possible implementation of SCALES is presented in detail.

The computational cost of implementing the SCALES methodology can be broken down into the cost of wavelet filtering to define the adaptive grid and the cost of the adaptive solver. The cost of the second generation wavelet filter is $O(N)$, i.e., of the same order as the adaptive wavelet collocation solver.[24,25] Note that the SCALES methodology could also be implemented using other suitable adaptive solvers.

IX. CONCLUSIONS

In this paper we have presented the theoretical basis for a new method for simulating turbulent flows called stochastic coherent adaptive large eddy simulation (SCALES) that attempts to combine the strengths of CVS and LES. The SCALES methodology uses the idea of wavelet threshold filtering the turbulent field as in CVS,[20] but in SCALES the wavelet filter threshold is increased so only the most energetic part of the coherent vortices are simulated in the resolved field. We have shown in this work that with both LES filtering and SCALES filtering the residual SGS field contains both coherent and incoherent parts. Also we have shown that the total SGS dissipation in both LES and SCALES is dominated by the coherent part of the SGS field.

This paper introduces a novel coherency diagram of a turbulent field that is useful in understanding the physical relationships between different large eddy capturing methods. The coherency diagram is used to present the physical relationships between direct numerical simulation and LES, VLES, and SCLES, which use Fourier filtering and are nonadaptive, and CVS and SCALES that use wavelet filtering and are fully adaptive.

Ongoing work on this project includes the development of a fully adaptive wavelet collocation solver that is considered ideal for implementing the SCALES methodology. We are also working on developing SGS stress models that will explicitly model the coherent and incoherent parts of the subgrid scale stress.

ACKNOWLEDGMENTS

The authors would like to thank Dr. Thomas Gatski at NASA Langley for his support of this work through a NASA GSRP fellowship for the first author of this paper. We would also like to thank Dr. David A. Yuen at the University of Minnesota Supercomputing Institute for his support of this work. Partial support for the second author (O.V.V.) was provided by the National Science Foundation under Grant Nos. EAR-0242591, EAR-0327269 and ACI-0242457. Computing time was provided by the NASA Ames Research Center, National Center for Supercomputing Applications, and Minnesota Supercomputing Institute and is gratefully acknowledged.

APPENDIX A: IMPLEMENTATION

Here we will outline a possible implementation of the SCALES methodology for incompressible turbulent flows. The actual implementation is the subject of future research. One can begin by applying the wavelet filter to the incompressible Navier–Stokes (NS) equations to obtain

$$\frac{\partial \overline{u_i}^{>\epsilon}}{\partial t} + \frac{\partial(\overline{u_i u_j}^{>\epsilon})}{\partial x_j} = -\frac{\partial \overline{p}^{>\epsilon}}{\partial x_i} + \nu \frac{\partial^2 \overline{u_i}^{>\epsilon}}{\partial x_j \partial x_j} + \mathcal{CE}, \quad \text{(A1)}$$

where $\mathcal{CE}$ is the commutation error,

$$\mathcal{CE}=-\underbrace{\left[\frac{\overline{\partial(u_iu_j)}^{>\epsilon}}{\partial x_j}-\frac{\partial(\overline{u_iu_j}^{>\epsilon})}{\partial x_j}\right]}_{NL\mathcal{CE}}+\underbrace{\left[\nu\frac{\overline{\partial^2u_i}^{>\epsilon}}{\partial x_j\partial x_j}-\nu\frac{\partial^2\overline{u_i}^{>\epsilon}}{\partial x_j\partial x_j}\right]}_{DIS\mathcal{CE}}$$
$$-\underbrace{\left[\frac{1}{\rho}\frac{\overline{\partial p}^{>\epsilon}}{\partial x_i}-\frac{1}{\rho}\frac{\partial\bar{p}^{>\epsilon}}{\partial x_i}\right]}_{P\mathcal{CE}}. \tag{A2}$$

For now we take the commutation error to be small and ignore it. Equation (A1) is still under resolved on the filtered grid because it relies on the unfiltered u_i in the nonlinear term. So as in LES we will introduce the SGS forcing term that will be modeled,

$$\frac{\partial\overline{u_i}^{>\epsilon}}{\partial t}+\frac{\partial(\overline{u_i}^{>\epsilon}\overline{u_j}^{>\epsilon})}{\partial x_j}=-\frac{\partial L_{ij}}{\partial x_j}-\frac{\partial\tau_{ij}}{\partial x_j}-\frac{1}{\rho}\frac{\partial\overline{p}^{>\epsilon}}{\partial x_i}+\nu\frac{\partial^2\overline{u_i}^{>\epsilon}}{\partial x_j\partial x_j}, \tag{A3}$$

where

$$L_{ij}=\overline{\overline{u_i}^{>\epsilon}\overline{u_j}^{>\epsilon}}^{>\epsilon}-\overline{u_i}^{>\epsilon}\overline{u_j}^{>\epsilon} \tag{A4}$$

is the Leonard stress and

$$\tau_{ij}=\overline{u_iu_j}^{>\epsilon}-\overline{\overline{u_i}^{>\epsilon}\overline{u_j}^{>\epsilon}}^{>\epsilon}. \tag{A5}$$

Up to this point it seems as if we are doing LES with a different type of filter but it is important to remember that the wavelet filter is being used to adapt the computational grid at every time step to track the most energetic vortices.

Now because the wavelets that we will be using are not divergence free vector wavelets the right-hand side of Eq. (A3) will not be divergence free. Also since the adaptive wavelet collocation solver that we will use does not have spectral accuracy the right-hand side of Eq. (A3) would not be divergence free even if a divergence free filter was used and τ_{ij} was known exactly. To correct for both sources of error in continuity a pressure corrector step[39] can be used. Then the adaptive wavelet collocation solver discussed above can be used to solve Eq. (A1). The pressure corrector step can then be applied to enforce a divergence free field.

Although in this paper we do not discuss the solution of the wavelet filtered Naiver–Stokes equation, it is important to point out that since the SCALES method uses an adaptive grid we cannot use spectral methods for the solution of the Poisson equation that arises in the pressure corrector step. The development of an efficient wavelet collocation based method for the solution of this Poisson equation on an adaptive grid is currently a subject of study.

APPENDIX B: SUBGRID SCALE DISSIPATION

As discussed above one of the advantages of the velocity formulation of the wavelet filter is the ability to calculate the SGS dissipation $\tau_{ij}S_{ij}$. But with a nondivergence free wavelet filter S_{ij} will not be trace free and therefore will be nonphysical for incompressible flow. For this reason we reformulated our equations to be able to find the SGS dissipation for this work.

To satisfy continuity the wavelet filtering operation must use a divergence free wavelet basis or a divergence free projection must be applied after the wavelet filtering operation. We will define our filtering operation as

$$\overline{u_i}^{>\epsilon}=\overline{u_i}^{>\epsilon\mathcal{P}}+(u_i)^{\phi}, \tag{B1}$$

where $(\,)^{\mathcal{P}}$ is a divergence free projection operator and u_i^{ϕ} is the nondivergence free part of $\overline{u_i}^{>\epsilon}$. In the case of a divergence free wavelet basis $u_i^{\phi}=0$. It should be noted here that the divergence free projection operator can only be applied to a vector field. This also applies to any divergence free wavelet transform. If we apply the wavelet filter operation defined in Eq. (B1) to the incompressible NS equations we get

$$\frac{\overline{\partial u_i}^{>\epsilon\mathcal{P}}}{\partial t}+\frac{\partial(u_i)^{\phi}}{\partial t}=\underbrace{\left[-\frac{\partial(\overline{u_i}^{>\epsilon\mathcal{P}}\overline{u_j}^{>\epsilon\mathcal{P}})}{\partial x_j}-\frac{\partial L_{ij}}{\partial x_j}-\frac{\partial\tau_{ij}}{\partial x_j}-\frac{1}{\rho}\frac{\partial\overline{p^*}^{>\epsilon}}{\partial x_i}+\nu\frac{\partial^2\overline{u_i}^{>\epsilon\mathcal{P}}}{\partial x_j\partial x_j}\right]}_{\mathcal{A}}+\underbrace{\left[\nu\frac{\partial^2(u_i)^{\phi}}{\partial x_j\partial x_j}\right]}_{\mathcal{B}} \tag{B2}$$

where

$$L_{ij}=\overline{\overline{u_i}^{>\epsilon\mathcal{P}}\overline{u_j}^{>\epsilon\mathcal{P}}}^{>\epsilon\mathcal{P}}-\overline{u_i}^{>\epsilon\mathcal{P}}\overline{u_j}^{>\epsilon\mathcal{P}}, \tag{B3}$$

and

$$\tau_{ij}=\overline{u_iu_j}^{>\epsilon}-\overline{\overline{u_i}^{>\epsilon\mathcal{P}}\overline{u_j}^{>\epsilon\mathcal{P}}}^{>\epsilon\mathcal{P}}. \tag{B4}$$

Then p^* is defined such that the terms in the first brackets on the right-hand side of Eq. (B2) ($\mathcal{A}$) are divergence free. Therefore the evolution of the divergence free velocity field is given by

$$\frac{\partial \overline{u_i}^{>\epsilon\mathcal{P}}}{\partial t}=\underbrace{\left[-\frac{\partial(\overline{u_i}^{>\epsilon\mathcal{P}}\overline{u_j}^{>\epsilon\mathcal{P}})}{\partial x_j}-\frac{\partial L_{ij}}{\partial x_j}-\frac{\partial \tau_{ij}}{\partial x_j}-\frac{1}{\rho}\frac{\partial \overline{p^*}^{>\epsilon}}{\partial x_i}+\nu\frac{\partial^2 \overline{u_i}^{>\epsilon\mathcal{P}}}{\partial x_j \partial x_j}\right]}_{\mathcal{A}}. \tag{B5}$$

The continuity equation [Eq. (B6)] is therefore satisfied for the divergence free wavelet filtered velocity $\overline{u_i}^{>\epsilon\mathcal{P}}$,

$$\frac{\partial \overline{u_i}^{>\epsilon\mathcal{P}}}{\partial x_i}=0. \tag{B6}$$

Finding the SGS dissipation is straightforward once we have derived the divergence free wavelet filtered Navier–Stokes equations [Eqs. (B5) and (B6)]. To find the SGS dissipation we will derive the kinetic energy transport equation by multiplying Eq. (B5) by $\overline{u_i}^{>\epsilon\mathcal{P}}$ (see Ref. 18),

$$\overline{u_i}^{>\epsilon\mathcal{P}}\left[\frac{\partial \overline{u_i}^{>\epsilon\mathcal{P}}}{\partial t}=-\frac{\partial(\overline{u_i}^{>\epsilon\mathcal{P}}\overline{u_j}^{>\epsilon\mathcal{P}})}{\partial x_j}-\frac{\partial L_{ij}}{\partial x_j}-\frac{\partial \tau_{ij}}{\partial x_j}-\frac{1}{\rho}\frac{\partial \overline{p^*}^{>\epsilon}}{\partial x_i}+\nu\frac{\partial^2 \overline{u_i}^{>\epsilon\mathcal{P}}}{\partial x_j \partial x_j}\right]. \tag{B7}$$

This results in the equation for the kinetic energy transport equation,

$$\frac{1}{2}\frac{\partial \overline{u_i}^{>\epsilon\mathcal{P}}\overline{u_i}^{>\epsilon\mathcal{P}}}{\partial t}=\underbrace{-\frac{\partial(\overline{u_i}^{>\epsilon\mathcal{P}}\overline{u_i}^{>\epsilon\mathcal{P}}\overline{u_j}^{>\epsilon\mathcal{P}})}{\partial x_j}}_{I}+\underbrace{L_{ij}\overline{S}_{ij}^{>\epsilon\mathcal{P}}}_{II}+\underbrace{\tau_{ij}\overline{S}_{ij}^{>\epsilon\mathcal{P}}}_{III}-\underbrace{\frac{\partial(\overline{u_i}^{>\epsilon\mathcal{P}}\tau_{ij})}{\partial x_j}}_{IV}$$
$$\underbrace{-\frac{1}{\rho}\frac{\partial \overline{u_i}^{>\epsilon\mathcal{P}}\overline{p^*}^{>\epsilon}}{\partial x_i}}_{V}+\underbrace{\frac{1}{2}\frac{\partial}{\partial x_j}\left(\nu\frac{\partial \overline{u_i}^{>\epsilon\mathcal{P}}\overline{u_i}^{>\epsilon\mathcal{P}}}{\partial x_j}\right)}_{VI}-\underbrace{\nu\frac{\partial \overline{u_i}^{>\epsilon\mathcal{P}}}{\partial x_j}\frac{\partial \overline{u_i}^{>\epsilon\mathcal{P}}}{\partial x_j}}_{VII} \tag{B8}$$

where

$$\overline{S}_{ij}^{>\epsilon\mathcal{P}}=\frac{1}{2}\left[\frac{\partial \overline{u_i}^{>\epsilon\mathcal{P}}}{\partial x_j}+\frac{\partial \overline{u_j}^{>\epsilon\mathcal{P}}}{\partial x_i}\right] \tag{B9}$$

and τ_{ij} is defined in Eq. (B4). The term III in Eq. (B8) is the SGS dissipation.

[1] P. Moin and J. Kim, "Tackling turbulence with supercomputers," Sci. Am. **276** (1), 62 (1997).
[2] J. Jimenez and P. Moin, "The minimal flow unit in near-wall turbulence," J. Fluid Mech. **225**, 213 (1991).
[3] P. A. Durbin and B. A. Pettersson Reif, *Statistical Theory and Modeling for Turbulent Flows* (Wiley, New York, 2001).
[4] G. H. Cottet and P. D. Koumoutsakos, *Vortex Methods: Theory and Applications* (Cambridge University Press, Cambridge, 2000).
[5] C. Canuto, M. Y. Hussaini, A. Quarteroni, and T. A. Zang, *Spectral Methods in Fluid Dynamics*, Springer Series in Comput. Phys. (Springer, New York, 1987).
[6] T. J. R. Hughes, L. Mazzei, and K. Jansen, "Large eddy simulation and the variational multiscale method," Comput. Vis. in Sci. **3**, 47 (2000).
[7] M. Lesieur and O. Métais, "New trends in large-eddy simulations of turbulence," Annu. Rev. Fluid Mech. **28**, 45 (1996).
[8] C. Meneveau and J. Katz, "Scale-invariance and turbulence models for large-eddy simulation," Annu. Rev. Fluid Mech. **32**, 1 (2000).
[9] P. Moin, "Advances in large eddy simulation methodology of complex flows," Int. J. Heat Fluid Flow **23**, 710 (2002).
[10] A. G. Kravchenko, P. Moin, and R. Moser, "Zonal embedded grids for numerical simulations of wall-bounded turbulent flows," J. Comput. Phys. **127**, 412 (1996).
[11] U. Piomelli, "Large-eddy simulation: Achievements and challenges," Prog. Aerosp. Sci. **35**, 335 (1999).
[12] J. Jimenez, A. Wray, P. Saffman, and R. Rogallo, "The structure of intense vorticity in isotropic turbulence," J. Fluid Mech. **225**, 65 (1993).
[13] D. E. Goldstein, O. V. Vasilyev, A. A. Wray, and R. S. Rogallo, "Evaluation of the use of second generation wavelets in the coherent vortex simulation approach," in *Proceedings of the 2000 Summer Program* (Center for Turbulence Research, Stanford, 2000), pages 293–304.
[14] M. Farge, G. Pellegrino, and K. Schneider, "Coherent vortex extraction in 3D turbulent flows using orthogonal wavelets," Phys. Rev. Lett. **87**, 054501 (2001).
[15] M. Farge and K. Schneider, "Coherent vortex simulation (CVS), a semi-deterministic turbulence model using wavelets," Flow, Turbul. Combust. **66**, 393 (2001).
[16] A. Vincent and M. Meneguzzi, "The spacial structure and statistical properties of homogeneous turbulence," J. Fluid Mech. **225**, 1 (1991).
[17] M. Germano, U. Piomelli, P. Moin, and W. H. Cabot, "A dynamic subgrid-scale eddy viscosity model," Phys. Fluids A **3**, 1760 (1991).
[18] S. B. Pope, *Turbulent Flows* (Cambridge University Press, Cambridge, 2000).
[19] M. Wang and P. Moin, "Dynamic wall modeling for large-eddy simulation of complex turbulent flows," Phys. Fluids **14**, 2043 (2002).
[20] M. Farge, K. Schneider, and N. Kevlahan, "Non-Gaussianity and coherent vortex simulation for two-dimensional turbulence using an adaptive orthogonal wavelet basis," Phys. Fluids **11**, 2187 (1999).
[21] W. Sweldens, "The lifting scheme: A custom-design construction of biorthogonal wavelets," Appl. Comput. Harmon. Anal. **3**, 186 (1996).

[22]W. Sweldens, ''The lifting scheme: A construction of second generation wavelets,'' SIAM J. Math. Anal. **29**, 511 (1998).
[23]O. V. Vasilyev and C. Bowman, ''Second generation wavelet collocation method for the solution of partial differential equations,'' J. Comput. Phys. **165**, 660 (2000).
[24]O. V. Vasilyev, ''Solving multidimensional evolution problems with localized structures using second generation wavelets,'' Int. J. Comput. Fluid Dyn. Special issue on High-resolution Methods in Computational Fluid Dynamics, **17**, 151 (2003).
[25]O. V. Vasilyev and N. K.-R. Kevlahan, ''Hybrid wavelet collocation—Brinkman penalization method for complex geometry flows,'' Int. J. Numer. Methods Fluids **40**, 531 (2002).
[26]N. K.-R. Kevlahan, O. V. Vasilyev, D. E. Goldstein, and A. Jay, ''A three-dimensional adaptive wavelet method for fluid-structure interaction,'' Technical University of Munich, Germany, 2003.
[27]I. Daubechies, ''Orthonormal bases of compactly supported wavelets,'' Commun. Pure Appl. Math. **41**, 909 (1988).
[28]A. Cohen, I. Daubechies, and J. Feauveau, ''Bi-orthogonal bases of compactly supported wavelets,'' Commun. Pure Appl. Math. **45**, 485 (1992).
[29]I. Daubechies, *Ten Lectures on Wavelets*, No. 61, in CBMS-NSF Series in Applied Mathematics (SIAM, Philadelphia, 1992).
[30]S. G. Mallat, *A Wavelet Tour of Signal Processing* (Academic, Paris, 1999).
[31]D. L. Donoho, ''Interpolating wavelet transforms,'' Technical Report No. 408, Department of Statistics, Stanford University, 1992.
[32]K. Schneider, N. Kevlahan, and M. Farge, ''Comparison of an adaptive wavelet method and nonlinearly filtered pseudo-spectral methods for two dimensional turbulance,'' Theor. Comput. Fluid Dyn. **9**, 191 (1997).
[33]N. K. R. Kevlahan and M. Farge, ''Vorticity filaments in two dimensional turbulence: Creation, stability, and effect,'' J. Fluid Mech. **346**, 49 (1997).
[34]D. Donoho, ''Unconditional bases are optimal bases for data compression and for statistical estimation,'' Appl. Comput. Harmon. Anal. **1**, 100 (1993).
[35]O. V. Vasilyev, T. S. Lund, and P. Moin, ''A general class of commutative filters for LES in complex geometries,'' J. Comput. Phys. **146**, 105 (1998).
[36]G. De Stefano and O. V. Vasilyev, ''Sharp cut-off vs smooth filtering in LES,'' Phys. Fluids **14**, 362 (2002).
[37]A. K. M. F. Hussain, ''Coherent structures and turbulence,'' J. Fluid Mech. **173**, 303 (1986).
[38]B. Cantwell, ''Organized motion in turbulent flow,'' Annu. Rev. Fluid Mech. **13**, 457 (1981).
[39]J. C. Tannehill, D. A. Anderson, and R. H. Pletcher, *Computational Fluid Mechanics and Heat Transfer* (Taylor and Francis, Washington, DC, 1997).